The Relationship between Sea Surface Temperature and Thermocline Depth in the Eastern Equatorial Pacific

HEIN ZELLE

KNMI, De Bilt, and DEOS, Delft, Netherlands

GERRIAN APPELDOORN, GERRIT BURGERS, AND GEERT JAN VAN OLDENBORGH

KNMI, De Bilt, Netherlands

(Manuscript received 26 February 2002, in final form 27 August 2003)

ABSTRACT

The time dependence of the local relation between sea surface temperature (SST) and thermocline depth in the central and eastern equatorial Pacific Ocean is analyzed for the period 1990–99, using subsurface temperature measurements from the Tropical Atmosphere–Ocean Array/Triangle Trans-Ocean Buoy Network (TAO/TRITON) buoy array. Thermocline depth anomalies lead SST anomalies in time, with a longitude-dependent delay ranging from 2 weeks in the eastern Pacific to 1 year in the central Pacific. The lagged correlation between thermocline depth and SST is strong, ranging from $r > 0.9$ in the east to $r \approx 0.6$ at 170°W. Time-lagged correlations between thermocline depth and subsurface temperature anomalies indicate vertical advection of temperature anomalies from the thermocline to the surface in the eastern Pacific. The measurements are compared with the results of forced OGCM and linear model experiments. Using model results, it is shown that the delay between thermocline depth and SST is caused mainly by upwelling and mixing between 140° and 90°W. Between 170°E and 140°W the delay has a different explanation: thermocline depth anomalies travel to the eastern Pacific, where upwelling creates SST anomalies that in turn cause anomalous wind in the central Pacific. SST is then influenced by these wind anomalies.

1. Introduction

The interactions that drive the El Niño–Southern Oscillation (ENSO) are sketched in Fig. 1. Sea surface temperature is chosen as a starting point along the cycle: large sea surface temperature variations, mostly in the eastern equatorial Pacific, change the strength of the trade winds, mainly in the center of the Pacific. The change in wind stress influences the local sea surface temperature directly by means of anomalous zonal advection, Ekman pumping (upwelling of cold water), evaporative cooling, and mixing. Also, it produces planetary (Kelvin) waves, which influence the depth of the thermocline. The change in thermocline depth leads to a change in sea surface temperature in the east by upwelling and mixing, completing the cycle. Negative feedback is provided by Rossby waves generated in the east, traveling to the western coast where they reflect as downwelling Kelvin waves, reversing the process. Suarez and Schopf (1988) and Battisti and Hirst (1989) describe this feedback loop as a delayed oscillator. A discussion of important mechanisms for El Niño variability is given in the review of Dijkstra and Burgers (2002).

In the ENSO cycle as described above, sea surface temperature (SST) and thermocline depth play important roles. SST anomalies are the manifestation of an El Niño event, while thermocline depth anomalies mark the onset and ending of an El Niño event.

According to previous studies, the two most important mechanisms influencing SST in the equatorial Pacific are zonal advection of mean temperature by anomalous zonal currents (often called zonal advective feedback) and mean vertical advection of subsurface temperature anomalies (often called thermocline feedback). The importance of thermocline feedback is stressed in the concepts of the delayed oscillator (Battisti and Hirst 1989; Suarez and Schopf 1988) and the recharge oscillator model (Jin 1997). Anomalous zonal advection and vertical advection are two of the most important terms in the SST equation of the Zebiak–Cane model (Zebiak and Cane 1987). Kleeman (1993) finds that thermocline depth changes have the strongest influence on SST in a coupled model, while zonal advection has a smaller influence. Picaut et al. (1996) stress the influence of zonal advection on SST in the equatorial Pacific in their analysis of Tropical Ocean and Global Atmosphere/

Corresponding author address: Hein Zelle, KNMI, P.O. Box 201, 3730 AE De Bilt, Netherlands.
E-mail: zelle@knmi.nl

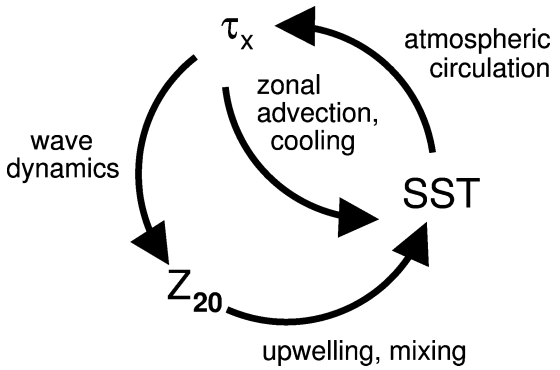

FIG. 1. The main feedbacks in the ENSO cycle: Z_{20} denotes the thermocline depth and τ_x is the zonal wind stress.

Tropical Atmosphere–Ocean Array (TOGA/TAO) measurements. Jin and An (1999) confirm, in a study using National Centers for Environmental Prediction–National Center for Atmospheric Research (NCEP–NCAR) reanalysis data and a simple recharge oscillator model, that anomalous zonal advection and mean vertical advection are the essential mechanisms that influence SST. They find that the influence of mean vertical advection is restricted to the eastern Pacific, while zonal advection influences mostly the central Pacific but also the eastern Pacific. Kang et al. (2001) use a budget study of NCEP–NCAR reanalysis data to investigate the relative importance of the various terms in the SST budget. They derive a simplified SST equation for ENSO, in which mean upwelling ($\overline{w}T_z'$) and anomalous zonal advection ($u'\overline{T}_x$) are the main contributing terms. Upwelling is dominant between 140° and 90°W on the equator, and is found to be most important during the mature phase of El Niño, while during the developing phase zonal advection and upwelling are equally important. Wang and McPhaden (2000, 2001) perform a similar study of mechanisms influencing SST in the equatorial Pacific, based on TAO/Triangle Trans-Ocean Buoy Network (TRITON) observations at four locations along the equator, for the 1997–98 El Niño. They also find that zonal advection is important in the central Pacific and that vertical advection is important in the eastern Pacific. The influence of zonal advection was mostly restricted to the onset of El Niño while vertical entrainment and diffusion were the most important processes during the termination phase. Vialard et al. (2001) have analyzed an OGCM forced by TAO/TRITON and *European Remote Sensing Satellites-1* and *-2* (*ERS1/2*) wind stress fields. They emphasize the importance of vertical advection and mixing in the eastern equatorial Pacific and of zonal advection in the western and and central equatorial Pacific. Mixing, a mechanism related to mean upwelling, is also emphasized as an important mechanism by Galanti and Tziperman (2002): subsurface temperature anomalies are transported vertically by mixing in the upper layer of the ocean. Fedorov and Philander (2001) use a stability analysis of a coupled ocean–atmosphere model to show how two unstable modes (one corresponding to the delayed oscillator and another associated with surface dynamics) with different behavior form the building blocks for ENSO. The second mode, associated with zonal advective feedback, is strongest in the central Pacific.

Other mechanisms play a role as well in the SST budget. Both anomalous advection of mean temperature and advection of anomalous temperature by mean current play a role in the zonal, meridional, and vertical directions, and surface fluxes are important as well. The budget study of Kang et al. (2001) provides useful maps of the relative importance of these mechanisms in the NCEP–NCAR reanalysis. They show that mean zonal advection ($\overline{u}T_x'$) is a small term except in the western Pacific. Anomalous meridional advection ($v'\overline{T}_y$) is also found to be a small term. Mean meridional advection ($\overline{v}T_y'$) can be a large term, especially during ENSO episodes when the eastern equatorial Pacific is very warm, and the meridional temperature gradient is high just off the equator. However, it effectively acts as a part of the Newtonian cooling term, only transporting excess heat away from the equator. Finally, they find that anomalous upwelling ($w'\overline{T}_z$) may be large at times in the eastern Pacific, but it is small on average compared to the mean upwelling term. Jin et al. (2003) show that the nonlinear upwelling term $w'T_z'$ is also important during strong events. Wang and McPhaden (2000, 2001) emphasize that there is not one dominating mechanism and that the relative importance of the mechanisms varies with the seasonal and ENSO cycles.

Harrison and Vecchi (2001) investigate the instantaneous correlation between thermocline depth and SST in the equatorial Pacific, using TAO/TRITON subsurface temperature data and NCEP gridded SST data. They only find a significant correlation in the eastern and east-central Pacific and conclude that SST anomalies cannot be attributed to thermocline depth anomalies.

Building on their work, the subject of this study is the time structure of the local relation between thermocline depth and SST in the central and eastern equatorial Pacific. There is a strong, time-lagged relationship between the two variables. By which pathways are thermocline depth anomalies connected to SST anomalies? Which mechanisms are involved in these pathways? What time scales are associated with the different mechanisms? Can we derive from the relation between thermocline depth and SST what the relative importance of the mechanisms is and where they are most important?

The starting point of our investigation is the lag correlation between observed thermocline depth anomalies and SST anomalies along the equator. This is shown in Fig. 2, using monthly subsurface temperature measurements from the TAO/TRITON array (McPhaden et al. 1998) from the period 1990–99. A monthly climatology was computed over this period and subtracted from the measurements to produce the anomalies. The depth of

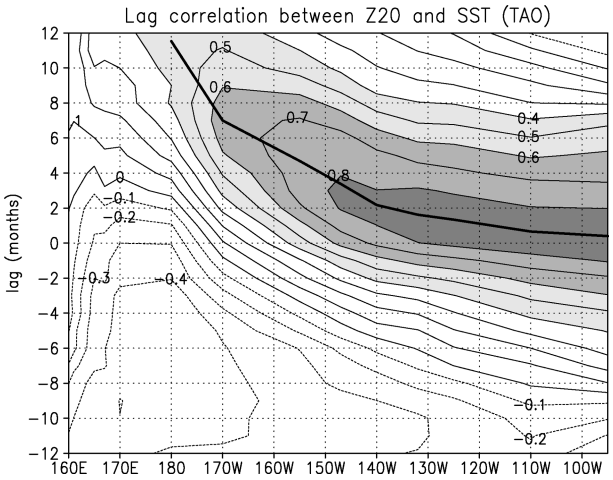

FIG. 2. Lag correlation between observed Z_{20} anomalies and SST anomalies on the equator. A positive lag means Z_{20} is leading SST. The correlation was computed using monthly temperature data from the TAO/TRITON array for the period 1990–99.

the 20°C isotherm is used as a proxy for the depth of the thermocline; it is denoted by Z_{20}. A similar but nonlocal correlation (between upper-ocean heat content and the Niño-3 index) is shown by Latif et al. (2001) in a comparison study of coupled ocean–atmosphere models.

Figure 2 depicts the time structure of the local relationship between SST and Z_{20} on the equator. The correlation between Z_{20} anomalies and SST anomalies is plotted as a function of longitude (horizontal axis) and lag (vertical axis). Contours show the strength of the correlation, while the thick line indicates the lag value where the correlation is maximal. Positive lag values mean that Z_{20} anomalies precede SST anomalies in time. There is a strong, direct relation ($r > 0.8$ at a lag of 2 weeks) between thermocline depth and SST in the eastern Pacific. In the central Pacific the relation is weaker ($r > 0.5$) and has a much larger lag ($\sim$12 months). In the western Pacific the relation is reversed, with SST anomalies leading Z_{20} variations by about 4 months ($r \approx -0.4$).

Apart from the TAO/TRITON subsurface temperature measurements, we make use of the output of a forced OGCM simulation to obtain variables that are not available from measurements, such as vertical velocities. To assess the importance of different mechanisms, a linear shallow-water model is used as well. It has a SST equation that can easily be modified, which makes it possible to test the importance of separate feedbacks by varying their strength without influencing other feedbacks.

The paper is organized as follows: in section 2, the observational data are described. The models and their outputs are described in section 3. In section 4 the observational data are analyzed, and it is explained how the models were used to analyze the mechanisms found in the measurements. Section 5 presents two pathways by which Z_{20} anomalies are linked to SST anomalies in the equatorial Pacific and discusses them in detail. A discussion of the analysis is presented in section 6, and the conclusions are listed in section 7.

2. Observations

For an investigation of the relation between Z_{20} and SST with observational data, measurements of Z_{20} and SST spanning several ENSO cycles are required. These measurements are available from the TAO/TRITON array, for the period from 1990 to the present (McPhaden et al. 1998).

The array consists of a set of buoys in the Pacific Ocean positioned at regular intervals on and around the equator. The buoys are positioned with a latitudinal spacing of 2° (8°S–8°N) and a longitudinal spacing of approximately 15°. Temperature measurements are performed at depths to 500 m at intervals of about 25 m from the surface to the thermocline. Both wind and air temperature measurements are performed at the surface.

We have converted the daily temperature observations to monthly means, filling gaps by linear interpolation where the time interval was shorter than 10 days. For wind measurements, the average of at least 10 daily measurements was used. These means were interpolated linearly in space to a regular grid. No interpolation was attempted if the vertical distance to a measurement was more than 10 m or 25%, the meridional distance was more than 1°, or the zonal difference was more than 10°. Also, values were not interpolated if the temperature difference was larger than 1 K. The depth of the 20°C isotherm (Z_{20}) was found by linear interpolation in the resulting dataset.

3. Model runs

Two models are used to complement the analysis of observational data. The first is an OGCM, used to provide quantities that are not directly measured, such as the upwelling velocity. The second model is a simple linear shallow-water model, used to analyze mechanisms involved in the problem.

a. HOPE

The Hamburg Ocean Primitive Equation Model (HOPE) is a general circulation ocean model. At the European Centre for Medium-Range Weather Forecasts (ECMWF) it is used for seasonal forecasts. The ocean model provides detailed fields of u, v, w, S, and T, which are reasonably realistic (Stockdale et al. 1998; van Oldenborgh et al. 1999). The vertical velocity is especially important since no adequate measurements of this quantity are available.

Details of the model physics and the applied numerical scheme are described in Wolff et al. (1997). The horizontal resolution of the model varies from 0.5°lat-

itude × 2.8° longitude at the equator, to 2.8° latitude × 2.8° longitude at midlatitudes. The upper 300 m of the ocean contain 10 depth levels; the deep ocean contains another 10. The model uses a shear-enhanced mixing scheme similar to that of Pacanowski and Philander (1981). In addition, a mixed layer is simulated by increasing the mixing to $D = 2 \times 10^{-3}\ \mathrm{m^2\ s^{-1}}$ when SST $- T_{\mathrm{sub}} < 0.5$ K.

A 10-yr hindcast run (1990–99) was performed, using daily ECMWF analysis fields of wind stress, heat flux, and freshwater flux as external forcing. The time period 1990–99 was chosen because of the availability of TAO/TRITON buoy measurements and model forcing fields. SST was relaxed to observations with a strength of 40 $\mathrm{W\ m^{-2}\ K^{-1}}$, weak enough to allow dynamical variability in the region of interest. However, east of 100°W, and to a lesser degree west of 170°E, HOPE simulates SST relatively poorly and relaxation has a significant effect. The simulation of Z_{20} is very good east of 160°W. West of the date line the quality of the Z_{20} simulation is somewhat reduced because of too-strong diffusion, but it remains good.

b. Linear shallow-water model

The linear model used in this study is a 1.5-layer shallow-water anomaly model of a baroclinic mode on a beta plane (Burgers et al. 2002) combined with a linear SST equation. The SST equation in the model has the following generic form:

$$\frac{dT}{dt} = \alpha(x)Z_{20}(x, y) + c\beta(x)\tau_x(x, y) - \gamma(x)T(x, y), \quad (1)$$

with T the SST anomaly field, Z_{20} the thermocline depth anomaly field, and τ_x the zonal wind stress forcing anomaly field. The equation consists of three terms. The first term is proportional to Z_{20}, representing mean upwelling of anomalous temperature. Kleeman (1993) uses a similar term in his model. The second term is proportional to τ_x, which is a proxy for zonal advection caused by zonal wind stress and other local effects. Latif (1987) describes this simple relationship between SST and wind stress and applies it in a conceptual model. The last term is a relaxation term proportional to T. The strength of the wind stress term can be changed with the constant factor c to determine the effect of a zonal wind stress coupling.

The model has a 2° zonal grid spacing and a 1° meridional grid spacing in a meridional domain of (30°S, 30°N). The model is forced with Florida State University (FSU) wind stress fields (Stricherz et al. 1997). Two model runs are performed. In the first run there is no local coupling between τ_x and SST: $c = 0$. In the second run τ_x and SST are coupled ($c = 1$). The strength of the coupling $\beta(x)$ varies with location depending on local climatological zonal wind stress and zonal temperature gradient conditions. Figure 3 shows the zonal dependence of the parameters α, β, and γ, subjectively tuned to obtain the best Niño-3 and Niño-4 simulations in forced runs when $c = 1$. Both model runs reproduce Niño-3 variability with high correlations between model results and observations in the eastern equatorial Pacific (Burgers and van Oldenborgh 2003).

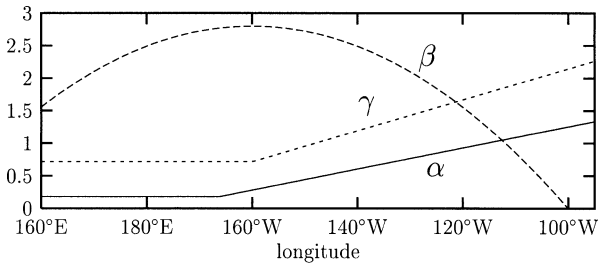

FIG. 3. Linear model parameters that determine the strength of various terms in the SST equation (arbitrary units).

4. Data analysis

a. Lag correlation between thermocline depth and SST, using TAO/TRITON data

Figure 2 shows there is a strong relationship between Z_{20} anomalies and SST anomalies along the equator. Between 180° and 90°W, the maximum correlation between Z_{20} and SST is in the range $0.5 < r < 0.9$. There is a gradually increasing time lag (maximum correlation line) between Z_{20} and SST anomalies when moving from 90°E toward the date line. Near the east coast the signal takes only 2 weeks to reach the surface, while near the date line there is a lag of almost a year between Z_{20} and SST anomalies. As the time lag increases, correlation values decrease. West of the date line the maximum correlation at positive lag is much lower ($r < 0.4$), indicating a different relationship between Z_{20} and SST in that region.

Further insight into the relationship between Z_{20} and SST is gained by plotting the correlation between Z_{20} anomalies and T_{sub} anomalies on the equator in a vertical cross section. Figure 4 shows such cross sections for the TAO/TRITON data for increasing lag values (again, a positive lag means Z_{20} leads SST). At lag 0 the thermocline is clearly visible as a band of very high correlations since thermocline depth anomalies are equivalent to local subsurface temperature anomalies. As time progresses, the line of high correlations moves up toward the surface, representing a temperature anomaly traveling from the thermocline to the surface. Across the whole section, correlation values are reduced in time, indicating the decay of the original thermocline depth signal. Note that at first strong signals ($r > 0.5$) only appear at the surface east of 160°W. After 4 months they also appear at 170°W, but never west of 180°. West of the date line there is little direct coupling between Z_{20} and SST: here Z_{20} anomalies and subsurface temperature anomalies are only coupled below 70–100 m.

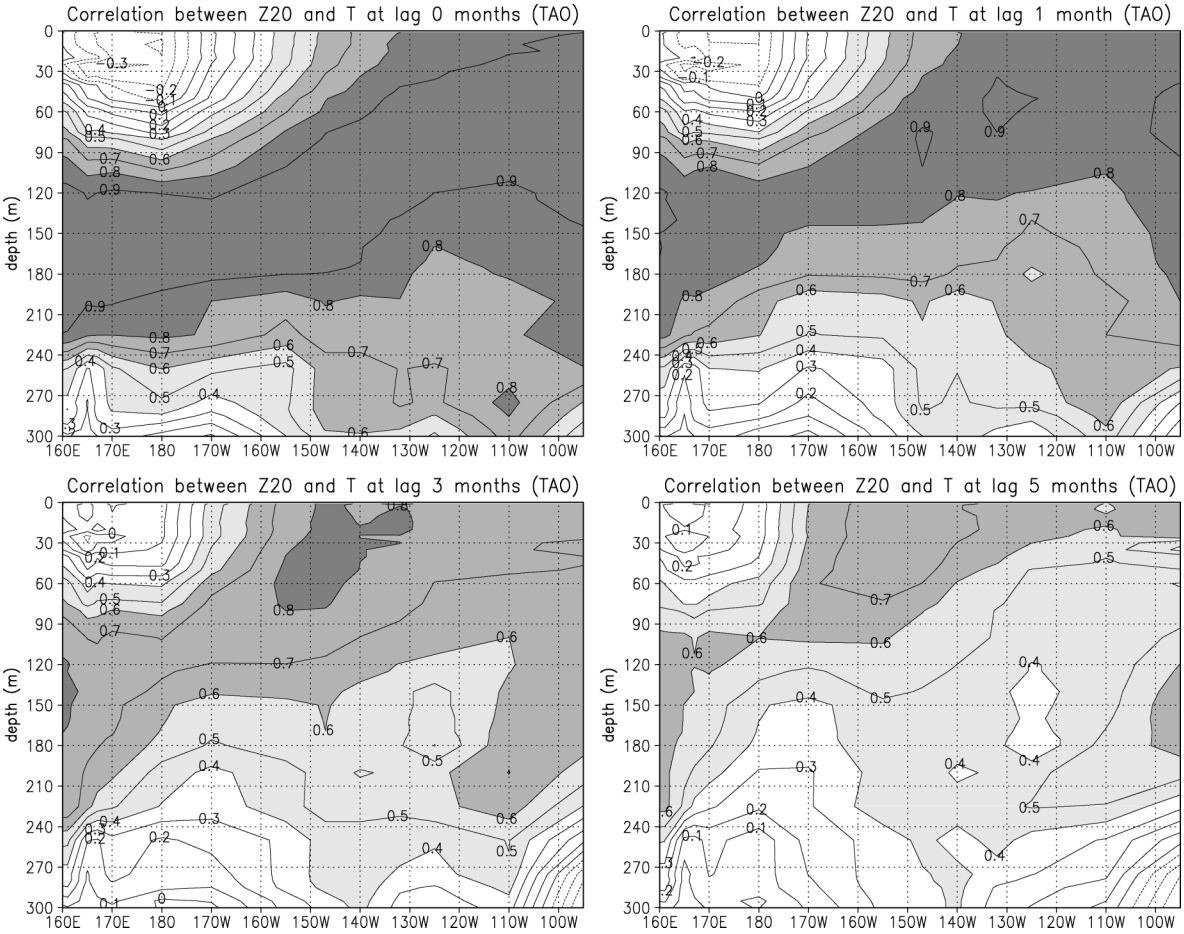

FIG. 4. Correlation between Z_{20} anomalies and T_{sub} anomalies on the equator (TAO/TRITON), for increasing lag values. A positive lag means Z_{20} is leading T_{sub}.

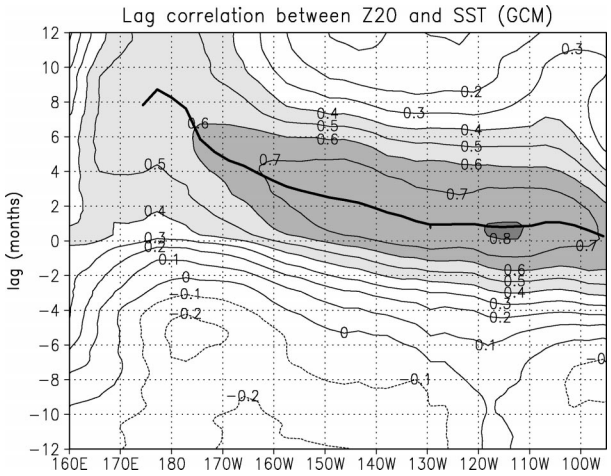

FIG. 5. Lag correlation between Z_{20} anomalies and SST anomalies on the equator for HOPE model output. A positive lag means Z_{20} is leading SST.

b. Lag correlation between thermocline depth and SST, using HOPE model output

The lag correlation between Z_{20} anomalies and SST anomalies in the HOPE model run is shown in Fig. 5. The model data compare reasonably well with the TAO/TRITON data; most features in the relation between Z_{20} and SST are present. The lag at which the correlation is maximal compares well in the eastern equatorial Pacific. Figure 6 shows these lags for TAO/TRITON data, HOPE model output, and the output of the linear shallow-water model described in section 3b. East of 145°W the comparison between HOPE and TAO/TRITON is good. Farther west HOPE starts to underestimate the lag with a maximum error of 4 months at 170°E. The maximum correlation values are about equal with correlations of around 0.8 between 150° and 100°W.

Figure 7 shows the same cross sections on the equator as in Fig. 4, this time taken from HOPE model output. The comparison with Fig. 4 is reasonable. East of the date line the correlations generally agree above the thermocline. West of the date line, HOPE underestimates the strength of the relation between Z_{20} and T_{sub} around

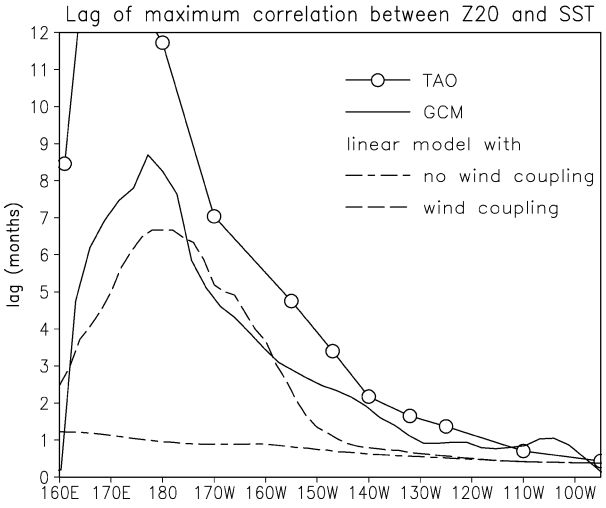

FIG. 6. Lag at which the correlation between Z_{20} anomalies and SST anomalies is maximal. This represents the time a Z_{20} anomaly needs to manifest itself as a SST anomaly.

the depth of the thermocline and overestimates the strength in the surface layer. Similar to the observations, HOPE does show an area west of the date line where the effects of Z_{20} anomalies do not penetrate to the surface, although the region is shallower (0–50 m) and lies farther west than in the observations.

The differences between HOPE results and observations in the western Pacific are probably related to too-strong mixing in HOPE around the thermocline in the western Pacific. Subsurface temperature profiles along the equator of the HOPE model run compare well with TAO/TRITON observations, but too strong mixing (and possibly upwelling) will cause a subsurface temperature response to thermocline anomalies too close to the surface. A comparison with Latif et al. (2001) shows that both in forced and coupled HOPE runs the lag between Z_{20} anomalies and SST response in the western Pacific is underestimated.

In conclusion, HOPE reproduces most features of the lag correlation between Z_{20} and SST in the central and eastern equatorial Pacific, and can be used for studying the mechanisms behind this relationship.

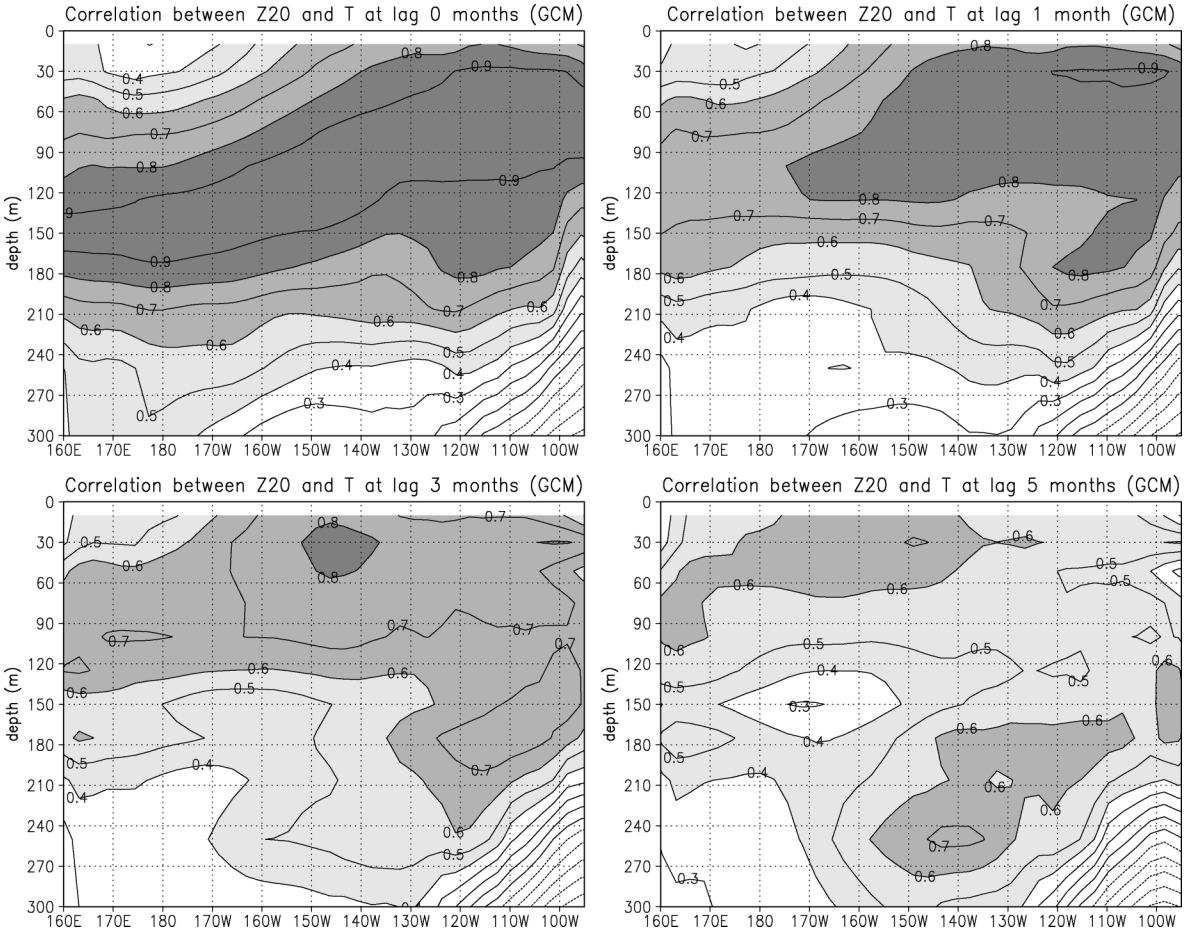

FIG. 7. Correlation between Z_{20} anomalies and T_{sub} anomalies on the equator (HOPE) for increasing lag values. A positive lag means Z_{20} is leading T_{sub}.

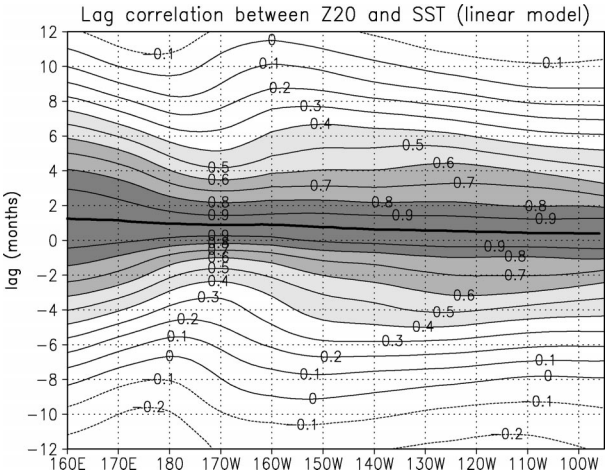

FIG. 8. Lag correlation between Z_{20} anomalies and SST anomalies on the equator for linear model output without wind stress coupling ($c = 0$). A positive lag means Z_{20} is leading SST.

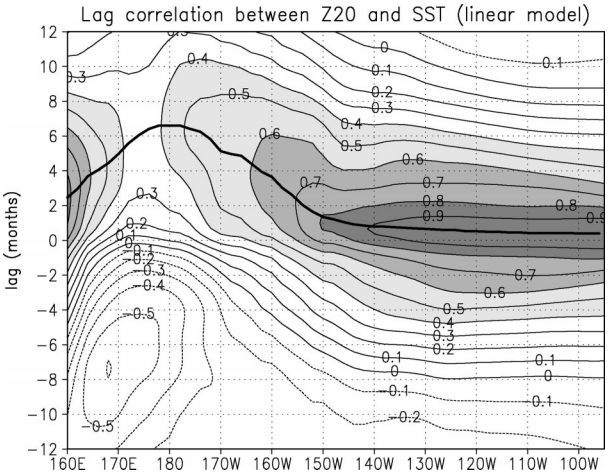

FIG. 9. Lag correlation between Z_{20} anomalies and SST anomalies on the equator for a linear model run with direct coupling between τ_x and SST ($c = 1$). A positive lag means Z_{20} is leading SST.

c. *Lag correlation between thermocline depth and SST using linear model output*

First the linear model run without local wind feedback ($c = 0$) is analyzed. Figure 8 shows the lag correlation between Z_{20} anomalies and SST anomalies as in Fig. 2. It is immediately clear that, in this configuration, the relation between Z_{20} and SST is described incorrectly by the linear model. Figure 6 shows the lag where the correlation has a maximum in comparison with TAO/TRITON and HOPE data. Farther east the lag is as observed, but it hardly increases toward the central Pacific.

The second linear model run, with local wind feedback ($c = 1$), performs much better. Figure 9 shows the lag correlation between Z_{20} anomalies and SST anomalies. The introduction of local τ_x–SST coupling clearly improves the situation in the east and central Pacific. Figure 6 shows that the simulation is still lacking in two respects: the increase in lag only appears west of 150°W, instead of 120°W, and the maximum lag value at 180° is 6 months, instead of 12 months, as observed in the TAO/TRITON data. The overall picture has improved considerably, however. There is an approximately linear relation between the strength of the wind coupling and the lag for values of c smaller than the default value $c = 1$. For higher values of c the lag increases more slowly. The model was tuned so that a value of $c = 1$ produces the best Niño-3 and Niño-4 simulations.

Figure 8 also sheds some light on the deficiencies of the HOPE model in the western Pacific. HOPE displays a lag between Z_{20} and SST anomalies that is too short, with too weak negative correlations at negative lags. The linear model without local wind coupling shows the same behavior, albeit more extreme. One could see it as the limiting case where vertical diffusion is infinitely strong: a thermocline depth anomaly translates directly into an SST tendency. Figures 8 and 5 suggest that in the western Pacific the HOPE simulation lies between this limiting case and observations: diffusion is too strong or the local wind coupling is too weak. Figure 6 shows that the time lag around the date line in HOPE is underestimated by around 3 months. This results in an ENSO cycle that is too short when HOPE is coupled to a statistical atmosphere, as described by van Oldenborgh et al. (1999). Latif et al. (2001) also find a too-short oscillation period in a coupled version of the HOPE model.

5. Two pathways

As discussed in the previous section, there is a clear relationship between Z_{20} and local SST in the TAO/TRITON data as well as the HOPE model run, especially east of 180°. Following a Z_{20} anomaly, a SST anomaly appears at the surface with a time delay depending on latitude. We discuss two pathways by which Z_{20} anomalies may lead to SST anomalies.

1) A Z_{20} anomaly is equivalent to a subsurface temperature anomaly T_{sub} at the level of the thermocline, which is transported upward by upwelling until it reaches the surface. Mixing also contributes to the vertical transport of temperature anomalies. This will be called the *upwelling pathway.* The upwelling pathway includes any SST feedback that is directly related to thermocline depth anomalies. It is a *local* pathway.
2) A downwelling Z_{20} anomaly travels from the central equatorial Pacific to the eastern Pacific where it causes a positive SST anomaly. This SST anomaly causes an eastward shift in the region of atmospheric convection above the equatorial Pacific and produces a westerly wind anomaly in the central Pacific. The wind anomaly drives anomalous eastward zonal advection across the temperature gradient in the central

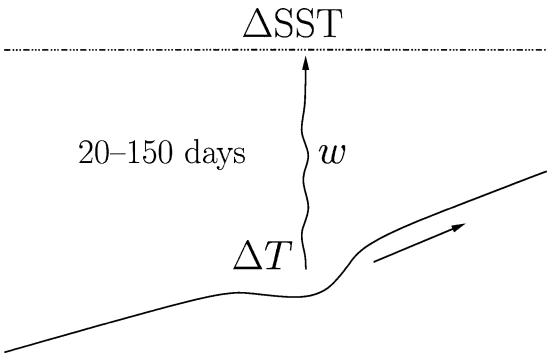

FIG. 10. Sketch of the upwelling pathway.

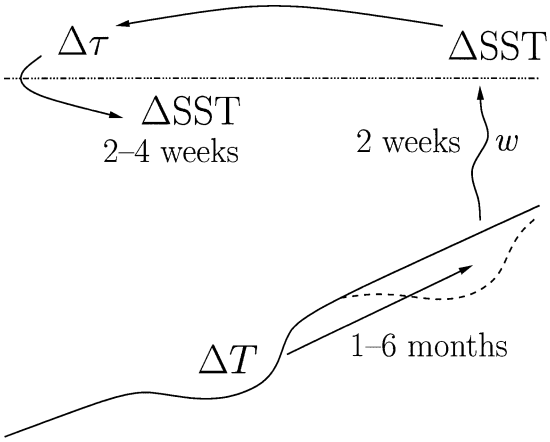

FIG. 11. Sketch of the wind coupling pathway.

Pacific, thereby causing a positive SST anomaly in the central Pacific. Also, the wind anomaly heats the surface waters directly through reduced evaporative cooling and reduced Ekman pumping, diminishing upwelling of colder subsurface waters. This pathway relies on wind feedbacks: local effects of anomalous wind on SST. It will be called the *wind coupling pathway*. Contrary to the upwelling pathway, a remote coupling through wave dynamics and an atmospheric response is required. This pathway is *nonlocal*: it makes an excursion to the eastern Pacific. Note that the upwelling pathway is included as a part of this pathway.

A passing Kelvin wave (Z_{20} anomaly) also induces anomalous zonal currents that, in the presence of a zonal temperature gradient, directly influence SST and T_{sub}. This effect is included in the correlation analysis, because it involves a local connection between Z_{20} and SST. It is similar to the upwelling pathway.

Figures 10 and 11 show schematic representations of these pathways. Their existence and importance will now be investigated in the two ocean models.

a. The upwelling pathway

Identifying the upwelling pathway is not easy since measurements of upwelling velocities are not readily available. Johnson et al. (2001) give an analysis of upwelling velocities computed from observed horizontal velocities and divergence in the equatorial Pacific. In an OGCM like HOPE however, the vertical velocity field w is explicitly modeled. In section 4 it was established that the HOPE OGCM reproduces most features of the Z_{20}–SST relationship in the central and eastern equatorial Pacific. The time scales of upwelling and mixing will be discussed, and an assessment of the importance of the upwelling pathway in HOPE (including mixing) for the relation between Z_{20} and SST is made.

The relevant time scales of upwelling and mixing in the relation between SST and Z_{20} depend on the depth of the mixed layer and the thermocline, respectively. For a given temperature profile $T(z)$, a proxy of the mixed layer depth Z_{mix} was determined by

$$\mathrm{SST} - T(Z_{mix}) = 0.5 \text{ K}.$$

The average depth of the mixed layer proxy (from HOPE model output) is shown in Fig. 12 and varies approximately from 50 m at 180° to 10 m at 120°W. Figure 12 also shows the average thermocline depth approximated by Z_{20}, which is about three times as deep as the mixed layer. Vertical sections on the equator are shown of the upwelling velocity and diffusion coefficient in the HOPE model output, averaged over the 10-yr period.

Using the model results, mixing and upwelling have been compared. Generally, in the HOPE model, mixing is a fast process when compared with upwelling in the upper mixed layer of the ocean and a slow process below the mixed layer. In the mixed layer, diffusion is the strongest process. In about 14 days, the typical penetration distance for diffusion ($\sqrt{Dt}$, $D \approx 2 \times 10^{-3}$ m^2 s^{-1}) is of the order of the mixed layer depth. Upwelling velocities reach maxima of about 2 m day^{-1} ($w \approx 2 \times 10^{-5}$ m s^{-1}) at the bottom of the mixed layer. Between the mixed layer and the thermocline, upwelling is the strongest process. Here, the penetration distance for diffusion is much smaller, of the order of 10 m in 14 days ($D \approx 10^{-4}$ m^2 s^{-1}).

To investigate the time scale of the upwelling pathway in HOPE, an estimate for the time lag between Z_{20} and SST anomalies calculated from upwelling velocities will be compared with the actual time lag found in the model run. First we consider the upwelling field w in HOPE. Figure 13 shows the mean upwelling velocity $\overline{w}$ and the standard deviation of w at the bottom of the mixed layer on the equator. Figure 13 shows a steady increase in $\overline{w}$ from 160°E to 160°W. Between 160° and 140°W $\overline{w}$ reaches a maximum value of 3×10^{-5} m s^{-1} ($\sim$2.6 m day^{-1}). This value is of the same order of magnitude as the $(1.9 \pm 0.9) \times 10^{-5}$ m s^{-1} reported by Johnson et al. (2001). Farther east $\overline{w}$ decreases strongly along the equator to a minimum at 100°W. (The upwelling zone is located farther south and continues along the South American coast.) The variability of w is large:

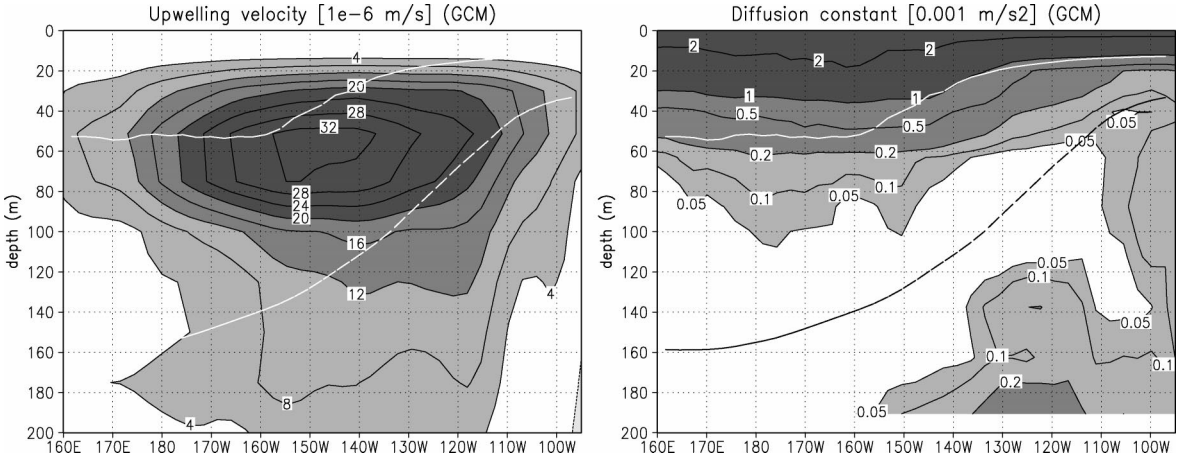

FIG. 12. Vertical sections on the equator of (left) vertical advection w and (right) diffusion coefficient D in the HOPE model. Values were time averaged over the 10-yr period. Both figures show the average mixed layer depth (upper line) and thermocline depth (lower line) in HOPE.

the standard deviation of w has the same order of magnitude as the mean $\overline{w}$ across the equatorial Pacific.

One would expect that, if upwelling were the only term involved in the relationship between Z_{20} and SST, the lag would be directly related to the upwelling velocity and thermocline depth. Higher upwelling velocities would give rise to shorter lags, while a deeper thermocline would imply longer lags. Figure 2 indeed shows an increasing time lag when moving west from 90°W. To see if this increasing lag corresponds to the local upwelling velocities and increasing thermocline depth, the expected lag is computed from the model output as

$$\Delta t_w = \int_{Z_{20}}^{0} \frac{1}{\overline{w}(z) + w_d(z)}\, dz. \qquad (2)$$

An effective vertical velocity component representing diffusion, w_d, is crudely estimated as follows: the penetration depth by diffusion is $z = \sqrt{Dt}$, and we take the time derivative to estimate a ''velocity'' w_d. Substituting $w_d = z/t$ leads to the approximation $w_d(z) = D/2z$. This correction to w is only important in the mixed layer.

The integral in Eq. (2) is dominated by the mean upwelling term. The next step is to compare this ''lag caused by upwelling'' with the actual lag found in the model output (Fig. 6). The lags are plotted in Fig. 14. They compare well in the east (140°–90°W, lag up to 2 months), while farther westward (180°–140°W) the modeled lag is larger (by up to 3 months) than the computed lag for upwelling. West of the date line, the longitudinal dependence of the modeled and the computed lag is quite different. The effect of anomalous upwelling has been left out of the analysis presented

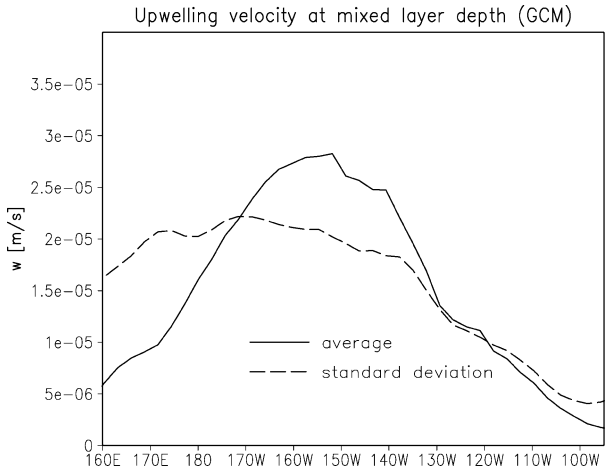

FIG. 13. Mean upwelling velocity $\overline{w}$ (m s^{-1}) in the HOPE model run, at the bottom of the mixed layer along the equator.

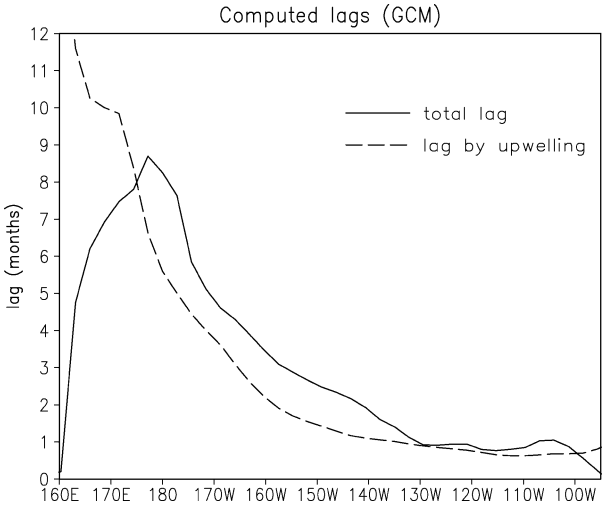

FIG. 14. Time lag between Z_{20} signal and SST response. Comparison of observed lag with computed lag for upwelling, both using HOPE model output.

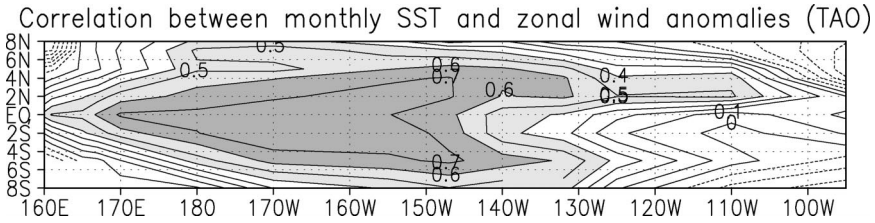

FIG. 15. Correlation between zonal wind anomalies and SST anomalies as computed from observed TAO/TRITON data (1990–99).

here. In the introduction it was noted that this term is small on average but may be large at times. The effect on the mean time lag Δt_w as presented in Fig. 14 is small (not shown). In certain cases the lag may increase because of reduced upwelling, like at the end of the 1997–98 El Niño, when zonal wind was reduced as far east as 100°W (McPhaden 1999). During La Niña the lag will be smaller.

The conclusion is that, in the HOPE model, mean upwelling of anomalous temperature is probably the most important pathway in the range 140°–90°W: it explains the observed lag of 2 weeks to 1 month between Z_{20} and SST. Farther west, a pathway other than upwelling is playing a role. The wind coupling pathway is the most likely cause: section 5b describes how wind coupling becomes more important in this region. Upwelling still contributes, but it is no longer the dominant pathway: it cannot explain the observed lag. The wind coupling pathway must be slower than the upwelling pathway: time lags increase rapidly where the wind coupling becomes more important.

b. The wind coupling pathway

We will try to verify the existence and importance of the wind coupling pathway using the TAO/TRITON data and with the aid of a simple linear model.

A simple way to illustrate that zonal wind has a strong influence on local SST in the equatorial Pacific is to plot the correlation between the two using TAO/TRITON measurements. Figure 15 shows that zonal wind has a strong coupling with SST in the range 170°E–140°W. The correlation between Niño-3 and zonal wind in the central equatorial Pacific is also high (not shown). The causal relationships behind these correlations are as follows: in the western Pacific SST is directly influenced by local zonal wind anomalies, while SST anomalies in the eastern Pacific are the cause of these wind anomalies. This corresponds with the previous section where it was expected that west of 140°W a pathway other than upwelling becomes important. On the equator, the correlation between meridional wind and SST is very weak (not shown).

To see if a zonal wind coupling can indeed introduce lags of 9–12 months in the central equatorial Pacific, the two linear model runs without and with direct wind–SST coupling (Figs. 8 and 9) are compared. The introduction of the wind coupling pathway increases the lag around the date line from about 1 month to 6–8 months (the maximum correlation in Fig. 9 occurs at a lag of 6 months, but at a lag of 8 months correlation values are almost identical). Although the lag in the central Pacific is shorter than observed, the linear model now has a lag structure similar to that of HOPE, even in the western Pacific, contrary to the computed lag for the upwelling pathway in Fig. 14. East of 140°W the lag structure does not improve because the upwelling pathway is dominant there. This shows that a coupling between zonal wind and SST can indeed produce lag correlation patterns similar to the observations in the central equatorial Pacific.

The total response time for the upwelling pathway (Fig. 10) varies from 14 days far in the east to 150 days at the date line. Based on the speed of a Kelvin wave, which is $\sim$2.5 m s^{-1}, the total time for the wind coupling pathway (Fig. 11) would vary between 65 days (140°W) and 85 days (180°). This may appear to be an inconsistency: an 85-day lag cannot explain the observed lag of 250 days at the date line (see Fig. 6). It was just shown, however, that direct wind coupling *can* produce such lags (of $\sim$8 months) in a simple model. How can this apparent inconsistency be explained?

When a free Kelvin wave departs from the central Pacific, it will indeed arrive at the east coast in 1–2 months where it will produce SST anomalies within 2 weeks. However, generally Z_{20} anomalies are not part of a free Kelvin wave, as discussed, for example, in the review by Neelin et al. (1998). Consider the shallow-water equation for zonal advection (e.g., Gill 1982):

$$\frac{\partial u}{\partial t} - fv + \frac{\partial \eta}{\partial x} = \tau_x. \tag{3}$$

On the equator ($f = 0$), τ_x is balanced by $\partial u/\partial t + \partial \eta/\partial x$. In a linear model, zonal current changes only when there is an imbalance between zonal wind stress and the slope of the thermocline. As discussed by Neelin et al. (1998), Z_{20} anomalies will propagate as a forced Kelvin wave: in an approximate balance between thermocline depth slope and zonal wind stress. The coupled system travels eastward at a much slower rate than the free Kelvin wave speed.

This explains how the lag associated with the wind coupling pathway can be as long as 250 days (Fig. 6).

A second explanation for the large observed lag in the linear model could be westward propagation of SST anomalies accompanied by a westward shift of zonal wind anomalies, as described by Neelin (1991). However, although episodes of westward SST propagation occur, diagrams of the lagged correlation between local SST and SST at 120°W show no systematic westward propagation of SST anomalies.

One might argue that the models used in this study do not simulate the full wind coupling pathway as described in section 5. Because the models are forced by observed surface winds, there is no simulated atmospheric response to SST anomalies in the eastern Pacific, breaking the connection between Z_{20} anomalies and SST anomalies in the central Pacific. A coupled version of the linear model (Burgers and van Oldenborgh 2003) shows the same behavior however, indicating that the observed lag between Z_{20} and SST anomalies in the central Pacific is, indeed, caused by the interaction between Kelvin waves, SST anomalies in the eastern Pacific, and the wind response to those anomalies.

6. Discussion

A comparison with previous studies shows that our results generally agree with earlier work. The strong simultaneous correlation between Z_{20} and SST that Harrison and Vecchi (2001) find in the eastern Pacific is confirmed. However, in the central Pacific *lagged* correlations are much stronger than nonlagged correlations. The present study shows that SST anomalies as far west as 140°W can be partially attributed to local Z_{20} anomalies, a result that does not follow from the analysis of Harrison and Vecchi (2001).

In section 5a it was shown that the upwelling pathway is dominant in the range 140°–90°W, while in section 5b it was shown that west of 140°W the wind coupling pathway is most important. Using the two main influences on SST, the thermocline feedback and the wind feedback, we have constructed these pathways by which local SST can be related to local Z_{20}. The two pathways are sufficient to explain the structure of the lag correlation between SST and Z_{20} anomalies. The areas of influence of the feedbacks needed to obtain this result are consistent with the results of Kang et al. (2001), Vialard et al. (2001), and others mentioned in the introduction, who agree that mean upwelling is the most important contribution to SST in the eastern equatorial Pacific, while farther west anomalous zonal advection (caused by wind) is the most important.

Upwelling and zonal advection are not the only mechanisms that play a role in the two feedbacks. Mixing in the upper-ocean layer of the eastern Pacific, found to be important by Galanti and Tziperman (2002) and Vialard et al. (2001), is included in the thermocline feedback. Wang and McPhaden (2001) find that both zonal advection and vertical heat flux (anomalous upwelling) are important in the central Pacific; these mechanisms are included in the wind coupling feedback together with other local effects of wind on SST. Our results provide no information on seasonal dependence and ENSO phase dependence, such as the work of Wang and McPhaden (2001); it does however use observational data from a 10-yr time period showing that the pathways are valid in general and not just for the 1997–98 El Niño.

The thermocline feedback and wind coupling feedback discussed above are closely related to the SST and delayed oscillator modes described by Neelin (1991) and Fedorov and Philander (2001). Our work emphasizes the distinction between SST tendencies directly related to thermocline depth and those related to the local influence of wind on SST. The distinction between the two feedbacks provides a natural spatial separation between the central and eastern equatorial Pacific. This is different from the usual distinction between zonal advection and upwelling through the base of the mixed layer, which are both important across the central and eastern Pacific (Jin and An 1999; Wang and McPhaden 2000, 2001). Burgers and van Oldenborgh (2003) make a distinction similar to that in this paper, showing the importance of local wind feedback in the central Pacific for a realistic simulation of the ENSO cycle in a linear coupled model.

Figure 8 emphasizes that models that lack mechanisms that are vital to the ENSO cycle, such as those in the wind coupling feedback, will fail to reproduce the time structure of the relation between Z_{20} and SST. Comparing the lag correlation between Z_{20} and SST with actual measurements is a good test of the ENSO dynamics in a model, as it is sensitive to the balance between the two most important mechanisms that influence SST. The test has also been applied to the model of Zebiak and Cane (1987). In this model, neither the strength nor the time structure of the Z_{20}–SST correlation compare very well with observations, with toolow correlations in the central Pacific and no noticeable time lag between Z_{20} and SST. Latif et al. (2001) use a similar test, the correlation between upper-ocean heat content and the Niño-3 index, to compare a large number of coupled ocean–atmosphere models. The main difference between our test and the test of Latif et al. (2001) is that, because our test uses local SST, it is sensitive to the strength of the local wind feedback. This allows it to distinguish between linear model runs with and without wind feedback.

7. Conclusions

This study investigates the relationship between thermocline depth (Z_{20}) and SST in the equatorial Pacific. TAO/TRITON Z_{20} and SST measurements are strongly correlated ($r > 0.8$ far in the east, $r > 0.5$ as far west as the date line) at time lags between 2 weeks (90°W) and 12 months (180°). Two important pathways are distinguished that cause the relation between Z_{20} and SST:

the ''upwelling pathway'' (Fig. 10) and the ''wind coupling pathway'' (Fig. 11).

The upwelling pathway consists of vertical advection of temperature anomalies from the thermocline to the surface. These temperature anomalies are caused by thermocline depth anomalies and are transported to the surface by a combination of upwelling and vertical mixing. At the surface they appear as SST anomalies. The wind coupling pathway starts with a thermocline depth anomaly in the central Pacific that travels eastward as a set of Kelvin waves, causing SST anomalies in the eastern Pacific. These SST anomalies induce zonal wind anomalies in the central Pacific. The anomalous zonal winds cause SST anomalies through anomalous upwelling and evaporation and through anomalous zonal advection across the edge of the warm pool.

Using the output of the HOPE OGCM and a simple linear model, the relative importance of these pathways was investigated. A comparison of the lag observed in the HOPE model with a lag value computed from the upwelling velocity and thermocline depth shows that the upwelling pathway is most important in the region 140°–90°W. In this region, the lag between Z_{20} and SST ranges from 2 weeks to 2 months. Mean upwelling exists as far west as the date line in HOPE, but its influence is much smaller there because of a deeper thermocline. A test with the linear model where a local coupling between zonal wind stress and SST was introduced shows that the zonal wind coupling pathway is most important in the region 170°E–140°W. In this region, the lag between Z_{20} and SST ranges from 2 to 12 months. East of 140°W, there is no direct coupling between zonal wind and local SST. This is because the zonal wind shows little response to anomalous SST in the eastern Pacific. Another factor is the weaker zonal temperature gradient in the surface water. Considering the continuity of the increasing lag between Z_{20} and SST when moving westward from the east coast, it is most likely that west of 140°W the two pathways overlap, and zonal wind coupling slowly takes over from upwelling in importance.

The lagged relationship between Z_{20} and SST, as found in TAO/TRITON measurements, is shown to be modeled reasonably well by the HOPE OGCM. The linear model used in this study showed a much improved relationship after introduction of a direct coupling between zonal wind stress τ_x and SST. Both thermocline feedback and wind stress feedback are required for the linear model to properly simulate SST across the equatorial Pacific. A comparison of the time structure of the Z_{20}–SST relationship between ocean models and observations is shown to be a good test for ENSO models (both forced and coupled) that is sensitive to the strength of the mechanisms that influence SST. The use of such a test may contribute to the improvement of model El Niño simulations.

Acknowledgments. The research presented in this paper is supported by the Research Council for Earth and Life Sciences (ALW) of the Netherlands Organization for Scientific Research (NWO), and the Space Research Organization Netherlands (SRON).

REFERENCES

Battisti, D. S., and A. C. Hirst, 1989: Interannual variability in a tropical atmosphere–ocean model: Influence of the basic state, ocean geometry, and nonlinearity. *J. Atmos. Sci.,* **46,** 1687–1712.

Burgers, G., and G. J. van Oldenborgh, 2003: On the impact of local feedbacks in the central Pacific on the ENSO cycle. *J. Climate,* **16,** 2396–2407.

——, M. A. Balmaseda, F. C. Vossepoel, G. J. van Oldenborgh, and P. J. van Leeuwen, 2002: Balanced ocean-data assimilation near the equator. *J. Phys. Oceanogr.,* **32,** 2509–2519.

Dijkstra, H. A., and G. Burgers, 2002: Fluid dynamics of El Niño variability. *Annu. Rev. Fluid Mech.,* **34,** 531–558.

Fedorov, A. V., and G. S. Philander, 2001: A stability analysis of tropical ocean–atmosphere interactions: Bridging measurements and theory for El Niño. *J. Climate,* **14,** 3086–3101.

Galanti, E., and E. Tziperman, 2002: The equatorial thermocline outcropping—A seasonal control on the tropical Pacific ocean–atmosphere instability strength. *J. Climate,* **15,** 2721–2739.

Gill, A. E., 1982: *Atmosphere–Ocean Dynamics.* Academic Press, 662 pp.

Harrison, D., and G. A. Vecchi, 2001: El Niño and La Niña—Equatorial Pacific thermocline depth and sea surface temperature anomalies, 1986–98. *Geophys. Res. Lett.,* **28,** 1051–1054.

Jin, F.-F., 1997: An equatorial recharge paradigm for ENSO. Part I: Conceptual model. *J. Atmos. Sci.,* **54,** 811–829.

——, and S.-I. An, 1999: Thermocline and zonal advective feedbacks within the equatorial ocean recharge oscillator model for ENSO. *Geophys. Res. Lett.,* **26,** 2989–2992.

——, ——, A. Timmermann, and J. Zhao, 2003: Strong El Niño events and nonlinear dynamical heating. *Geophys. Res. Lett.,* **30,** 1120, doi:10.1029/2002GL016356.

Johnson, G. C., M. J. McPhaden, and E. Firing, 2001: Equatorial Pacific Ocean horizontal velocity, divergence, and upwelling. *J. Phys. Oceanogr.,* **31,** 839–849.

Kang, I.-S., S.-I. An, and F.-F. Jin, 2001: A systematic approximation of the SST anomaly equation for ENSO. *J. Meteor. Soc. Japan,* **79,** 1–10.

Kleeman, R., 1993: On the dependence of hindcast skill on ocean thermodynamics in a coupled ocean–atmosphere model. *J. Climate,* **6,** 2012–2033.

Latif, M., 1987: Tropical ocean circulation experiments. *J. Phys. Oceanogr.,* **17,** 246–263.

——, and Coauthors, 2001: ENSIP: The El Niño Simulation Intercomparison Project. *Climate Dyn.,* **18,** 255–276.

McPhaden, M. J., 1999: Genesis and evolution of the 1997–98 El Niño. *Science,* **283,** 950–954.

——, and Coauthors, 1998: The Tropical Ocean Global Atmosphere (TOGA) observing system: A decade of progress. *J. Geophys. Res.,* **103,** 14 169–14 240.

Neelin, J. D., 1991: The slow sea-surface temperature mode and the fast-wave limit: Analytic theory for tropical interannual oscillations and experiments in a hybrid coupled model. *J. Atmos. Sci.,* **48,** 584–606.

——, D. S. Battisti, A. C. Hirst, F.-F. Jin, Y. Wakata, T. Yamagata, and S. Zebiak, 1998: ENSO theory. *J. Geophys. Res.,* **103,** 14 261–14 290.

Pacanowski, R. C., and S. G. H. Philander, 1981: Parameterization of vertical mixing in numerical models of tropical oceans. *J. Phys. Oceanogr.,* **11,** 1443–1451.

Picaut, J., M. Ioulalen, C. Menkes, and T. Delcroix, 1996: Mechanism of the zonal displacement of the Pacific warm pool: Implications for ENSO. *Science,* **274,** 1486–1489.

Stockdale, T. N., D. L. T. Anderson, J. O. S. Alves, and M. A. Balmaseda, 1998: Global seasonal rainfall forecasts using a coupled ocean–atmosphere model. *Nature,* **392,** 370–373.

Stricherz, J., D. Legler, and J. O'Brien, 1997: *Pacific Ocean.* Vol. 2, *TOGA Pseudo-Stress Atlas 1985–1994,* The Florida State University, Tallahassee, FL, 158 pp.

Suarez, M. J., and P. S. Schopf, 1988: A delayed action oscillator for ENSO. *J. Atmos. Sci.,* **45,** 3283–3287.

van Oldenborgh, G. J., G. Burgers, S. Venzke, C. Eckert, and R. Giering, 1999: Tracking down the ENSO delayed oscillator with an adjoint OGCM. *Mon. Wea. Rev.,* **127,** 1477–1496.

Vialard, J., C. Menkes, J.-P. Boulanger, P. Delecluse, and E. Guilyardi, 2001: A model study of oceanic mechanisms affecting equatorial Pacific sea surface temperature during the 1997–98 El Niño. *J. Phys. Oceanogr.,* **31,** 1649–1675.

Wang, W., and M. J. McPhaden, 2000: The surface-layer heat balance in the equatorial Pacific Ocean. Part II: Interannual variability. *J. Phys. Oceanogr.,* **30,** 2989–3008.

——, and ——, 2001: Surface layer temperature balance in the equatorial Pacific during the 1997–98 El Niño and 1998–99 La Niña. *J. Climate,* **14,** 3393–3407.

Wolff, J.-O., E. Maier-Reimer, and S. Legutke, 1997: The Hamburg Ocean Primitive Equation model HOPE. Deutsches Klimarechenzentrum Tech. Rep. 13, Hamburg, Germany, 110 pp. [Available from Deutsches Klimarechenzentrum, Bundesstr. 55, D-20146 Hamburg, Germany.]

Zebiak, S. E., and M. A. Cane, 1987: A model of El Niño–Southern Oscillation. *Mon. Wea. Rev.,* **115,** 2262–2278.